

Dynamic phase separation of fluid membranes with rigid inclusions

Thomas R. Weikl*

Max-Planck-Institut für Kolloid- und Grenzflächenforschung, 14424 Potsdam, Germany

(Received 5 September 2002; published 30 December 2002)

Membrane shape fluctuations induce attractive interactions between rigid inclusions. Previous analytical studies showed that the fluctuation-induced pair interactions are rather small compared to thermal energies, but also that multibody interactions cannot be neglected. In this paper, it is shown numerically that shape fluctuations indeed lead to the dynamic separation of the membrane into phases with different inclusion concentrations. The tendency of lateral phase separation strongly increases with the inclusion size. Large inclusions aggregate at very small inclusion concentrations and for relatively small values of the inclusions' elastic modulus.

DOI: 10.1103/PhysRevE.66.061915

PACS number(s): 87.16.Dg, 64.75.+g, 05.10.Ln

I. INTRODUCTION

Biological and biomimetic membranes consist of a lipid bilayer with various types of macromolecules such as proteins [1,2]. Many of these macromolecules are incorporated in the bilayer, others are covalently bound or adsorbed to the membrane. The membranes are fluid and often tend to phase separate and form domains or “rafts” with different molecular compositions. In biological membranes, the presence of domains has been linked to specific functions in signaling [3], budding [4], or cell adhesion [5,6]. In some cases, the domain formation is caused by a separation of the lipid bilayer into phases with different lipid compositions [7,8]. In other cases, the phase separation of the membrane appears to be driven by attractive interactions between membrane inclusions [9].

Besides direct interactions such as van der Waals or electrostatic forces, membrane inclusions are subject to indirect interactions that are mediated by the membrane. Some of these membrane-mediated interactions are *static*, i.e., they arise from local perturbations of the bilayer structure or shape around the inclusions. Transmembrane proteins that exhibit a hydrophobic mismatch with respect to the lipid bilayer cause a perturbation of the bilayer thickness. This thickness perturbation has been found to induce attractive interactions between the proteins [10–13]. Similar interactions due to membrane thickness perturbations have also been proposed for adsorbed particles [14]. Membrane inclusions with conical shape [15–21] or membrane-anchored polymers [22,23] cause local perturbations of the membrane curvature, which induce attractive or repulsive interactions.

Other indirect interactions are *dynamic*, i.e., they are mediated by shape fluctuations of the membrane. In this paper, rigid membrane inclusions are considered, which interact due to the suppression of membrane shape fluctuations [15,24–30], see Fig. 1. Fluctuation-induced interactions have also been found for specific receptors or stickers that locally bind opposing membranes during adhesion [31–33].

The fluctuation-induced pair interactions of rigid membrane inclusions have been studied intensively [15,19,20,24–

27,30]. The pair interaction of rigid disks with radius r and distance L was found to be

$$G(L) = -6k_B T (r/L)^4 + O[(r/L)^6] \quad (1)$$

in the absence of an external membrane potential and lateral tension [15,26]. Here, $O[(r/L)^6]$ stands for terms of sixth or higher order in r/L . The prefactor of the leading term in Eq. (1) was first 12, and later corrected to 6 [26], see also Refs. [19,20,25,30]. Since the distance L has to be larger than the inclusion diameter $2r$, this term is only a fraction of the thermal energy $k_B T$. However, higher-order terms in (r/L) might be relevant at small inclusion separations, and thus contribute to the phase behavior of a membrane with many inclusions. Deducing the phase behavior of such a membrane is also complicated by nontrivial multi-body interactions [27].

In this paper, it is shown numerically that membrane-shape fluctuations indeed lead to the aggregation of rigid inclusions. The phase behavior of a discretized membrane with rigid inclusions is considered in Monte Carlo simulations. The membrane consists of quadratic patches with linear extension a , which corresponds to the smallest possible wavelength for bending deformations. Computer simulations of molecular membrane models indicate that this length scale is about 6 nm for a lipid bilayer with a thickness of about 4 nm [34]. Above a critical value K^* for the stiffness modulus of the inclusions, the membrane is found to separate into an inclusion-rich and an inclusion-poor phase. The aggregation tendency of the inclusions strongly increases with the size Q , which is reflected in a decrease of the critical stiffness K^* with the inclusion size. Large inclusions also aggregate already at relatively small inclusion concentrations. Here, quadratic inclusions with a size Q of 2×2 , 3×3 , or 4×4 mem-



FIG. 1. Rigid inclusion in the lipid bilayer.

*Electronic address: Thomas.Weikl@mpikg-golm.mpg.de

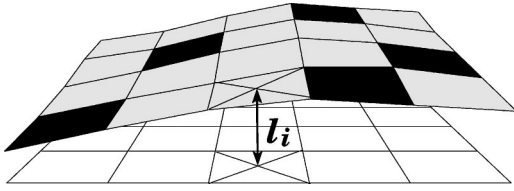


FIG. 2. A membrane segment containing inclusions with the size of one lattice site. The segment consists of 5×4 membrane patches that are labeled by the lattice sites i . Membrane patches with black inclusions correspond to occupation numbers $n_i=1$, while gray patches without inclusion have occupation numbers $n_i=0$. The local deviation of the membrane from the white reference plane is denoted by l_i .

brane patches are considered, which extends previous results on smaller inclusions with the size of a single patch [29]. For these inclusions, the critical stiffness is found to decrease according to the power law $K^* \sim Q^c$ with exponent $c \approx -0.70$.

II. GENERAL MODEL

The configurations of a fluctuating membrane with inclusions can be described by a field l for the membrane shape and a concentration field n for the inclusions [35]. For a membrane that is on average planar, the membrane shape is usually given by the deviation $l(x,y)$ from a reference plane with coordinates x and y . Here, the reference plane is discretized into a square lattice with lattice constant a , which corresponds to the smallest possible wavelength for bending deformations. The inclusion positions are then given by occupation numbers $n_i=0$ or 1 , where $n_i=1$ denotes the presence of an inclusion at the lattice site i of the reference plane, see Fig. 2.

In the absence of inclusions, the discretized bending energy per lattice site can be written as

$$\mathcal{E}_i^M(l) = \frac{1}{2} a^2 \kappa_o (c_{i,x} + c_{i,y})^2, \quad (2)$$

where κ_o is the bending rigidity of the lipid bilayer, and $\frac{1}{2}(c_{i,x} + c_{i,y})$ is the local mean curvature of the membrane [36]. Here,

$$c_{i,x} = (l_{x+a,y} + l_{x-a,y} - 2l_{x,y})/a^2, \quad (3)$$

$$c_{i,y} = (l_{x,y+a} + l_{x,y-a} - 2l_{x,y})/a^2, \quad (4)$$

are the discretized curvatures in x and y directions at the lattice site i with coordinates (x,y) . The rigid inclusions here are characterized by the elastic energy per site,

$$\mathcal{E}_i^I(l) = \frac{1}{2} a^2 K (c_{i,x}^2 + c_{i,y}^2), \quad (5)$$

with the stiffness modulus K [37]. For $K \rightarrow \infty$, such inclusions are completely rigid and suppress any local curvature at the inclusion position similar to the rigid disks or rods studied in Refs. [15,25,26,30]. In contrast, inclusions with increased bending rigidity as considered in Refs. [24,27,29] only suppress fluctuations of the total curvature $c_{i,x} + c_{i,y}$, but not saddle-type fluctuations with $c_{i,x} = -c_{i,y}$.

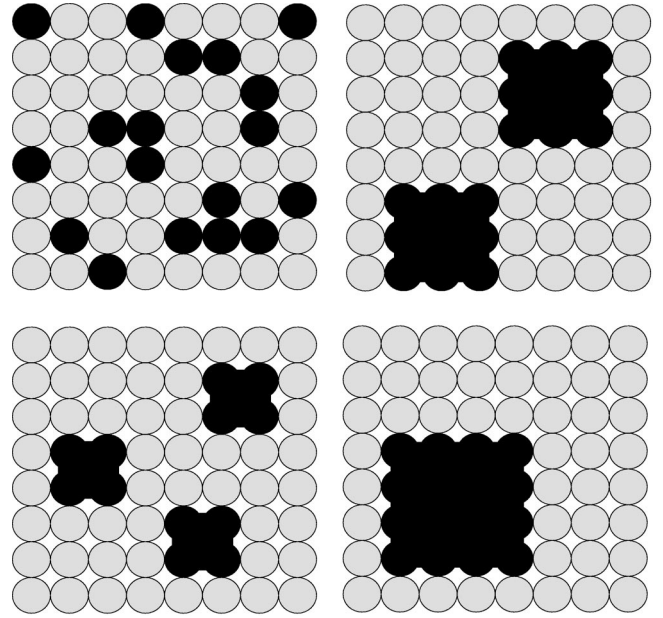


FIG. 3. Top view of membrane segments with inclusions of size $Q=1$, 2×2 , 3×3 , and 4×4 , respectively. The inclusions are shown in black.

The grand-canonical Hamiltonian of a membrane containing inclusions with the size of one lattice site can be written as

$$\mathcal{H}_{Q=1}\{l,n\} = \sum_i \{ (1-n_i) \mathcal{E}_i^M(l) + n_i [\mathcal{E}_i^I(l) - \mu] + V(l_i) \}, \quad (6)$$

where μ is the relative chemical potential of the inclusions and $V(l_i)$ is the external membrane potential. For lattice sites with occupation numbers $n_i=1$ indicating the presence of inclusions, the elastic energy is given by $\mathcal{E}_i^I(l)$. For lattice sites with $n_i=0$, the elastic energy is the energy $\mathcal{E}_i^M(l)$ of the lipid bilayer.

The larger inclusions considered here have an area of $Q=2 \times 2$, 3×3 , or 4×4 membrane patches or lattice sites, see Fig. 3. The elastic energy at every lattice site of an inclusion is given by Eq. (5). The larger inclusions thus can be seen as quadratic arrays of small inclusions with the size of one lattice site. The grand-canonical Hamiltonian for a membrane with larger inclusions can be formally written as [32]

$$\mathcal{H}_Q\{l,n\} = \sum_i \left\{ \mathcal{E}_i^M(l) + n_i \left[\sum_{q=1}^Q [\mathcal{E}_{i_q}^I(l) - \mathcal{E}_{i_q}^M(l)] - \mu \right] + V(l_i) \right\} + \sum_{\langle ij \rangle} W_{ij} n_i n_j, \quad (7)$$

where $\{i1, \dots, iQ\}$ denotes quadratic arrays of $Q=2 \times 2$, 3×3 , or 4×4 lattice sites. The position of an inclusion given by $n_i=1$ corresponds to one of the lattice sites occupied by the inclusion, e.g., the center of an inclusion with size $Q=3 \times 3$. The hard-square interaction

$$\begin{aligned}
 W_{ij} &= \infty \text{ for } j \text{ in } A_i^Q \\
 &= 0 \text{ otherwise}
 \end{aligned}
 \quad (8)$$

prevents any overlap of inclusions. Here, A_i^Q denotes the exclusion area of an individual inclusion with size Q at lattice site i .

In the following, the external potential of the membrane is taken to be the harmonic potential

$$V(l_i) = ml_i^2/2 \quad (9)$$

with potential strength m . The harmonic potential introduces an additional length scale, the correlation length $\xi = (4a^2\kappa_o/m)^{1/4}$ for the deviation field l , see, e.g., Ref. [24]. Membrane fluctuations on length scales larger than the correlation length ξ are suppressed by the harmonic potential, while fluctuations on smaller scales are governed predominantly by the elastic energy of the membrane.

The membrane model defined by Eqs. (2)–(7) has four characteristic dimensionless parameters, as can be shown by introducing the rescaled deviation field

$$z \equiv (l/a)\sqrt{\kappa_o/(k_B T)}. \quad (10)$$

These parameters are the ratio K/κ_o of the inclusion modulus and the bare membrane rigidity, the dimensionless chemical potential $\mu/(k_B T)$ for the inclusions, the rescaled potential strength $\tilde{m} \equiv ma^2/\kappa_o$, and the inclusion size Q .

III. MONTE CARLO SIMULATIONS

To deduce the phase behavior from Monte Carlo simulations, the inclusion concentration $X \equiv Q\langle n_i \rangle/a^2$ is determined as a function of the chemical potential μ for various values of the inclusion stiffness K , size Q , and the rescaled potential strength \tilde{m} . A first-order phase transition is reflected in a discontinuity of $X(\mu)$ at a certain chemical potential μ_{ir} . The two limiting values of $X(\mu)$ at μ_{ir} are the inclusion concentrations of the coexisting phases, an inclusion-rich and an inclusion-poor phase. To determine the inclusion concentration X at a given value of μ , Monte Carlo simulations are performed with up to 10^7 Monte Carlo steps per lattice site on a lattice with 120×120 sites and periodic boundary conditions. Each Monte Carlo step consists in attempted local moves of the rescaled deviation field z and of the concentration field n on all lattice sites. For rescaled potential strengths $\tilde{m} \geq 0.01$ as considered here, the correlation length of the membrane is much smaller than the lateral extension of the lattice, and finite size effects are negligible.

In Fig. 4, phase diagrams as a function of the inclusion modulus K are shown for inclusions with size $Q=1$, 2×2 , and 3×3 . The rescaled potential strength is $\tilde{m}=0.01$. At points (X, K) inside the shaded two-phase coexistence regions, the membrane separates into an inclusion-rich and an inclusion-poor phase. The inclusion concentrations in the coexisting phases are given by the lines of Monte Carlo data points, the critical points are represented by stars. The extent of the two-phase regions strongly increases with the inclu-

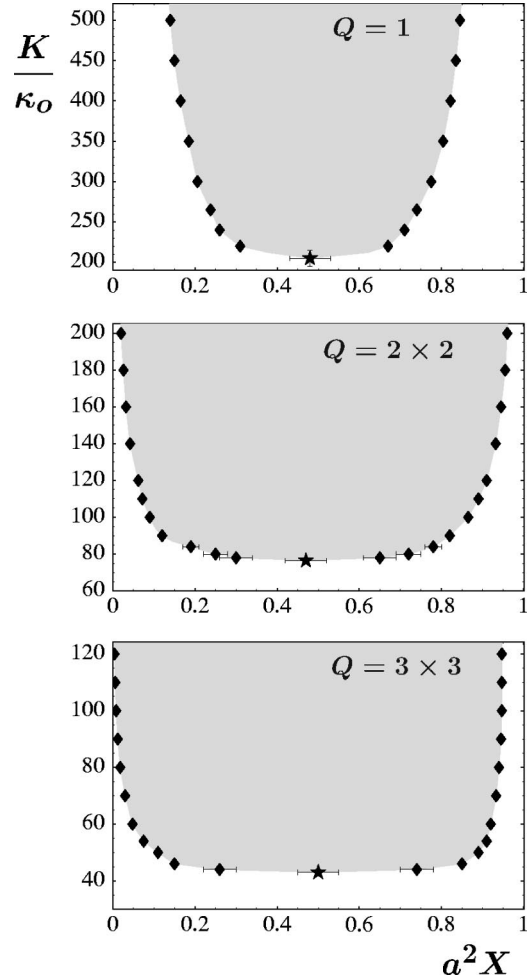


FIG. 4. Phase diagrams for inclusions with size $Q=1$, $Q=2 \times 2$, and $Q=3 \times 3$ as function of the inclusion concentration X and stiffness K in units of the bare membrane rigidity κ_o . The rescaled potential strength is $\tilde{m}=0.01$. Inside the shaded coexistence regions, the membrane separates into an inclusion-rich and an inclusion-poor phase with concentrations given by the lines of Monte Carlo points. The critical points are represented by stars.

sion size Q , which is reflected (i) in a strong decrease of the critical stiffness K^* and (ii) in an increase of the width of the coexistence region with the inclusion size. For inclusions with size $Q=3 \times 3$, the membrane phase separates already at very small inclusion concentrations.

The external harmonic potential (9) suppresses membrane-shape fluctuations for length scales larger than the correlation length $\zeta = a(4\tilde{m})^{1/4}$. Since the phase separation of the membrane is driven by the fluctuations, the critical stiffness K^* increases with the rescaled potential strength \tilde{m} , see Fig. 5. For weak potentials with small values of \tilde{m} , the critical stiffness is rather independent of \tilde{m} and tends towards a limiting value, since the correlation length ζ then is much larger than the average distance between neighboring inclusions.

In the absence of an external potential, i.e., for $\tilde{m}=0$, the critical stiffness K^* of the inclusions only depends on the inclusion size Q . Since the increasing correlation length ζ leads to finite size effects in Monte Carlo simulations with

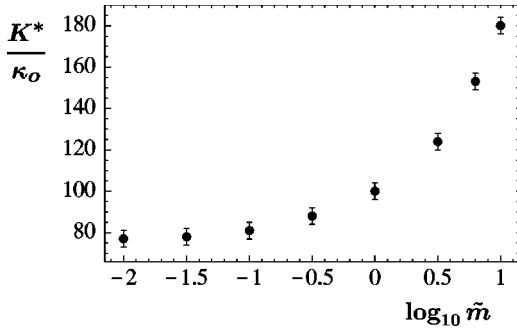


FIG. 5. Critical inclusion stiffness K^* as a function of the rescaled potential strength \tilde{m} for inclusions with size $Q=2\times 2$. The critical stiffness K^* is given in units of the bare membrane rigidity κ_o and increases with \tilde{m} since the harmonic potential suppresses membrane fluctuations.

$\tilde{m}=0$, the critical stiffness K^* for $\tilde{m}\rightarrow 0$ is determined here by extrapolation, see Table I. For the inclusion sizes considered in this paper, the functional dependence of the critical values K^* for $\tilde{m}\rightarrow 0$ on the size Q can be approximated by the power law

$$K^* \sim Q^c, \quad (11)$$

with exponent $c = -0.70 \pm 0.01$, see Fig. 6.

IV. SCALING ANALYSIS

Large inclusions with size $Q > 1$ can be seen as quadratic arrays of small inclusions with the size of one lattice site. These inclusions aggregate at much smaller values of the stiffness K than inclusions with size $Q=1$, see above. In order to understand this behavior, it is instructive to consider the free energy difference ΔF between the two membrane states: The uniform state in which the inclusions are more or less homogeneously distributed throughout the membrane and the phase-separated state in which the inclusions are aggregated. If ΔF is negative, the membrane will be in its homogenous state; if ΔF is positive, the membrane will phase separate. For a given area concentration X of the inclusions, the free energy difference between the uniform and the aggregated state can be written as

$$\Delta F(K, Q) = \Delta F_{int}(K, Q) - T\Delta S_{mix}(Q) \quad (12)$$

TABLE I. Critical values K^*/κ_o of the inclusion stiffness K in units of the bare membrane rigidity κ_o for various inclusion sizes Q and rescaled potential strengths \tilde{m} . Values for K^*/κ_o in the limit $\tilde{m}\rightarrow 0$ are obtained by extrapolation from the critical values at finite \tilde{m} shown in the columns 2–4.

	$\tilde{m}=1$	$\tilde{m}=0.1$	$\tilde{m}=0.01$	$\tilde{m}\rightarrow 0$
$Q=1$	300 ± 10	225 ± 10	205 ± 10	198 ± 10
$Q=2\times 2$	100 ± 2	81 ± 2	77 ± 2	76 ± 2
$Q=3\times 3$	55 ± 2	44 ± 2	43 ± 2	42.9 ± 2
$Q=4\times 4$	37 ± 2	29 ± 2	28 ± 2	27.9 ± 2

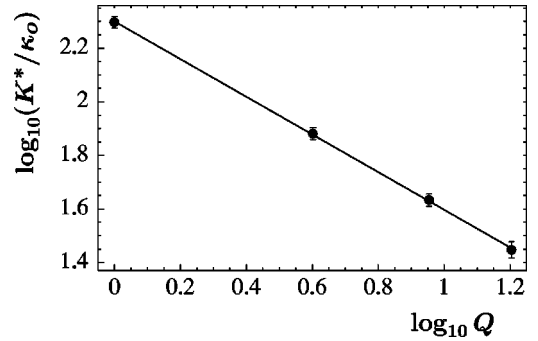


FIG. 6. Scaling plot for the critical inclusion stiffness K^* as a function of the size Q in the limit of the rescaled potential strength $\tilde{m}\rightarrow 0$, see also Table I. The straight line has the slope -0.70 , which corresponds to the exponent c in Eq. (11).

in the absence of an external potential, i.e., for $m=0$. Here, $\Delta F_{int}(K, Q)$ is the difference in the dynamic interaction free energy of the inclusions, which is induced by the shape fluctuations of the membrane, and $\Delta S_{mix}(K, Q)$ is the difference in the entropy of mixing.

The second term in Eq. (12) is dominated by the entropy of mixing in the homogeneous state. For small area concentrations $X = Q\langle n_i \rangle / a^2$ of the inclusions, this entropy of mixing is proportional to the number of inclusions, and ΔS_{mix} scales as

$$\Delta S_{mix}(Q) \sim 1/Q. \quad (13)$$

Equation (13) simply results from the fact that the number of inclusions is proportional to $1/Q$ for given area concentration X of the inclusions.

The term $\Delta F_{int}(K, Q)$ is dominated by the interaction free energy of the inclusions in the aggregated state. For $Q > 1$, the inclusions are rather densely packed in this state with an area fraction $a^2 X$ larger than 0.9 (see Fig. 4), and have contact with neighboring inclusions almost along the whole circumference of length $4\sqrt{Q}$. If one assumes that the interaction free energy in the aggregated state is proportional to the ratio of the inclusion circumference $4\sqrt{Q}$ and the area Q , the scaling form of the interaction free energy difference can be estimated as

$$\Delta F_{int}(K, Q) \approx f(K) / \sqrt{Q} \sim K^m / \sqrt{Q}, \quad (14)$$

presupposing power law form for $f(K)$. According to this estimate, the interaction free energy ΔF_{int} decreases with the inclusion size Q proportional to $Q^{-1/2}$, following the decrease of the “surface-to-area” ratio of the inclusions. The critical stiffness K^* obtained from $\Delta F=0$ then scales as

$$K^* \sim Q^{-1/(2m)}. \quad (15)$$

Comparing with the exponent $c \approx -0.70$ from the Monte Carlo simulations (see Fig. 6), one obtains

$$m = -1/(2c) \approx 0.71. \quad (16)$$

Thus, for the stiffness values K and inclusion sizes Q considered here, the dynamic interaction free energy ΔF_{int} of the inclusions appears to increase proportional to $K^{0.71}$.

V. DISCUSSION

In summary, I have considered the dynamic phase behavior of a discretized membrane with rigid inclusions using Monte Carlo simulations. The phase behavior strongly depends on the inclusion size. For inclusion sizes ranging from $Q=1$ to $Q=4 \times 4$ lattice sites or membrane patches, the critical stiffness K^* decreases with the size as $K^* \sim Q^{-0.70}$ in the absence of an external potential, see Fig. 6. The lateral extension of a membrane patch, the lattice spacing a , corresponds to the cutoff length for membrane-shape fluctuations, which has been estimated as 6 nm for a membrane with a thickness of about 4 nm [34]. In biological or biomimetic membranes, rigid objects with an extension larger than 6 nm may correspond to large transmembrane proteins, aggregates of proteins and other macromolecules, or, more general, membrane domains with increased elastic moduli. Colloidal particles adsorbed on membranes suppress membrane fluctuations similar to rigid inclusions. In general, membrane inclusions and membrane-adsorbed particles may have a variety of shapes and, therefore, orientational degrees of freedom [20,26,28]. Here, I have only considered quadratic objects on a square lattice. At high area concentrations $a^2 X > 0.8$, the phase behavior of the membrane with quadratic inclusions of size $Q > 1$ is complicated by the packing transitions of the hard-square lattice gas [38,39], which are not considered here. These transitions are induced by the hard-square interactions (8) of the inclusions, but do not depend on the inclusion stiffness in contrast to the dynamic phase separation.

The inclusions considered here suppress fluctuations of the local curvatures $c_{i,x}$ and $c_{i,y}$ in x and y directions at the inclusion sites, see Eqs. (3)–(5). In contrast, inclusions with increased bending rigidity studied in Refs. [24,27,29] only suppress fluctuations of the total curvature $c_{i,x} + c_{i,y}$, but not “saddle-type” fluctuations with $c_{i,x} = -c_{i,y}$, which seems somewhat less realistic. The phase behavior of these inclusions is remarkably different from that of the rigid inclusions

studied here. Inclusions with increased bending rigidity do not interact in the absence of an external membrane potential, since local fluctuations of the total curvature at different membrane sites are not correlated in the free membrane [24]. Such correlations are only induced by the external potential of the membrane. The fluctuation-induced interactions between inclusions with increased bending rigidity attain a maximum at a certain nonzero potential strength, but are always considerably weaker than those of rigid inclusions characterized by Eq. (5), see Ref. [29]. Intermediate cases between these two types of inclusions can be studied by using an elastic energy with two moduli for the inclusions [29].

Rigid inclusions may also be subject to other membrane-mediated interactions if they perturb the bilayer thickness or have a conical or wedgelike shape, see the Introduction. In general, dynamic fluctuation-induced interactions can be assumed to be additive to static interactions arising from perturbations of the equilibrium membrane structure, as long as these perturbations do not affect the elastic moduli of the membrane. The variety of membrane-mediated indirect interactions often complicates the interpretation of experimental results. The dynamic phase separation of a fluctuating multicomponent membrane in contact with a substrate has been recently reported in Ref. [40]. The membrane contains anchored polymers and appears to phase separate into domains with different separation from the substrate, which might result from different effective bending rigidities for the domains since the fluctuation-induced Helfrich repulsion [41] between membrane and substrate depends on the rigidity. Fluctuation-induced interactions may also contribute to the aggregation of latex spheres adsorbed to vesicles reported in Ref. [42]. Lateral phase separation has also been observed during the adhesion of biomimetic membranes with specific receptors or stickers that bind to ligands in a supported membrane [9]. Phase separation during membrane adhesion may be induced by membrane fluctuations [32,33] or by an effective barrier in the interaction energy between the membranes [33,43,44]. In the first case, the aggregation tendency of the stickers strongly increases with the sticker size, similar to the rigid inclusion considered here [32]. The fluctuation-induced interactions between bound stickers are also enhanced if the stickers are more rigid than the surrounding membrane [33].

-
- [1] B. Alberts *et al.*, *Molecular Biology of the Cell*, 3rd ed. (Garland, New York, 1994).
 - [2] R. Lipowsky and E. Sackmann, *The Structure and Dynamics of Membranes* (Elsevier, Amsterdam, 1995).
 - [3] K. Simons and E. Ikonen, *Nature (London)* **387**, 569 (1997).
 - [4] R. Schekman and L. Orci, *Science* **271**, 1526 (1996).
 - [5] C.R.F. Monks, B.A. Freiberg, H. Kupfer, N. Sciaky, and A. Kupfer, *Nature (London)* **395**, 82 (1998).
 - [6] A. Grakoui, S.K. Bromley, C. Sumen, M.M. Davis, A.S. Shaw, P.M. Allen, and M.L. Dustin, *Science* **285**, 221 (1999).
 - [7] S.L. Keller, W.H. Pitcher, III, W.H. Huestis, and H.M. McConnell, *Phys. Rev. Lett.* **81**, 5019 (1998).
 - [8] C. Dietrich, L.A. Bagatolli, Z.N. Volovyk, N.L. Thompson, M. Leve, K. Jacobson, and E. Gratton, *Biophys. J.* **80**, 1417 (2001).
 - [9] A. Albersdörfer, T. Feder, and E. Sackmann, *Biophys. J.* **73**, 245 (1997); A. Kloboucek, A. Behrisch, J. Faix, and E. Sackmann, *ibid.* **77**, 2311 (1999); Z. Guttenberg, B. Lorz, E. Sackmann, and A. Boulbitch, *Europhys. Lett.* **54**, 826 (2001).
 - [10] N. Dan, A. Berman, P. Pincus, and S. Safran, *J. Phys. II* **4**, 1713 (1994).
 - [11] J.-B. Fournier, *Europhys. Lett.* **43**, 725 (1998).
 - [12] S. May and A. Ben-Shaul, *Biophys. J.* **76**, 751 (1999).
 - [13] T.A. Harroun, W.T. Heller, T.M. Weiss, L. Yang, and H.W. Huang, *Biophys. J.* **76**, 937 (1999).
 - [14] P. Schiller, *Phys. Rev. E* **62**, 918 (2000); *Mol. Phys.* **98**, 493 (2000).

- [15] M. Goulian, R. Bruinsma, and P. Pincus, *Europhys. Lett.* **22**, 145 (1993); **23**, 155(E) (1993).
- [16] T.R. Weigl, M.M. Kozlov, and W. Helfrich, *Phys. Rev. E* **57**, 6988 (1998).
- [17] K.S. Kim, J. Neu, and G. Oster, *Biophys. J.* **75**, 2274 (1998); *Europhys. Lett.* **48**, 99 (1999).
- [18] T. Sintes and A. Baumgärtner, *J. Phys. Chem. B* **102**, 7050 (1998).
- [19] P.G. Dommersnes and J.-B. Fournier, *Europhys. Lett.* **46**, 256 (1999).
- [20] P.G. Dommersnes and J.-B. Fournier, *Eur. Phys. J. B* **12**, 9 (1999).
- [21] P. Biscari and F. Bisi, *Eur. Phys. J. E* **7**, 381 (2002); P. Biscari, F. Bisi, and R. Rosso, *J. Math. Biol.* **45**, 37 (2002).
- [22] M. Breidenich, R.R. Netz, and R. Lipowsky, *Europhys. Lett.* **49**, 431 (2000).
- [23] T. Bickel, C. Marques, and C. Jeppesen, *Phys. Rev. E* **62**, 1124 (2000); T. Bickel, C. Jeppesen, and C.M. Marques, *Eur. Phys. J. E* **4**, 33 (2001).
- [24] R.R. Netz and P. Pincus, *Phys. Rev. E* **52**, 4114 (1995).
- [25] J.-M. Park and T.C. Lubensky, *J. Phys. I* **6**, 1217 (1996).
- [26] R. Golestanian, M. Goulian, and M. Kardar, *Europhys. Lett.* **33**, 241 (1996); *Phys. Rev. E* **54**, 6725 (1996).
- [27] R.R. Netz, *J. Phys. I* **7**, 833 (1997).
- [28] R. Holzlöhner and M. Schoen, *Eur. Phys. J. B* **12**, 413 (1999).
- [29] T.R. Weigl, *Europhys. Lett.* **54**, 547 (2001).
- [30] W. Helfrich and T.R. Weigl, *Eur. Phys. J. E* **5**, 423 (2001).
- [31] R. Bruinsma, M. Goulian, and P. Pincus, *Biophys. J.* **67**, 746 (1994).
- [32] T.R. Weigl, R.R. Netz, and R. Lipowsky, *Phys. Rev. E* **62**, R45 (2000).
- [33] T.R. Weigl and R. Lipowsky, *Phys. Rev. E* **64**, 011903 (2001).
- [34] R. Goetz, G. Gompper, and R. Lipowsky, *Phys. Rev. Lett.* **82**, 221 (1999).
- [35] R. Lipowsky, *Phys. Rev. Lett.* **77**, 1652 (1996).
- [36] W. Helfrich, *Z. Naturforsch. C* **28**, 693 (1973).
- [37] The rigid inclusions with modulus K characterized by Eq. (5) correspond to the “stiff” inclusions considered in Ref. [29] with moduli $\kappa = \hat{\kappa}$.
- [38] L.K. Runnels, *Phase Transitions and Critical Phenomena*, edited by C. Domb and M.S. Green (Academic Press, New York, 1972), Vol. 2.
- [39] W. Kinzel and M. Schick, *Phys. Rev. B* **24**, 324 (1981).
- [40] S. Marx, J. Schilling, E. Sackmann, and R. Bruinsma, *Phys. Rev. Lett.* **88**, 138102 (2002).
- [41] W. Helfrich, *Z. Naturforsch. A* **33**, 305 (1978).
- [42] I. Koltover, J.O. Rädler, and C.R. Safinya, *Phys. Rev. Lett.* **82**, 1991 (1999).
- [43] S. Komura and D. Andelman, *Eur. Phys. J. E* **3**, 259 (2000); T.R. Weigl, D. Andelman, S. Komura, and R. Lipowsky, *ibid.* **8**, 59 (2002).
- [44] R. Bruinsma, A. Behrisch, and E. Sackmann, *Phys. Rev. E* **61**, 4253 (2000).